Unified Power Flow Controller for PV Systems Using AI-Driven Power Quality Improvement Using Coupled Inductor Dual Boost Converter

[1]Chindam A., [1]IlanjiAkilandam C., [2]DugyalaV.
[1]Annamalai University, Chidambaram India
[2]Kamala Institute of Technology and Science, Telangana, India.

Abstract. Voltage stability, power flow regulation, and Power Quality have become major issues as a result of the increasing integration of renewable energy sources, especially photovoltaic (PV) systems, into power transmission networks. The main objective of this research is to improve the power quality (PQ) in power system utilizing Renewable Energy Sources (RESs), notably by eliminating the harmonic content in voltage and current that arise from power electronics interfaces. To address this, a Unified Power Flow Controller (UPFC), is proposed comprising both series and shunt converters interlinked with DC-link capacitor. In addition, a Photovoltaic (PV) system is integrated with a Coupled Inductor Dual Boost (CIDB) converter to ensure a stable and continuous energy supply. To accomplish these objectives, a Coyote Optimized Radial Basis Function Neural Network (COA-RBFNN) based Maximum Power Point Tracking (MPPT) is adopted for ensuring efficient energy extraction from PV system. Furthermore, a Decoupled Neural Network (DNN) based control technique is integrated to manage UPFC efficiently. The research is modelled and simulated in Matlab. The most important results of the study demonstrate a significant improvement in improving PQ, even under changing load conditions. Moreover, the converter ranks with improved efficiency of 88%, with improved voltage and current characteristics. The significance of the results is found in the ability to integrate renewable energy with contemporary power control technologies while guaranteeing dependable and high-quality power delivery.

Keywords: power quality (PQ), PV, Coupled Inductor Dual Boost converter, Coyote Optimized RBFNN MPPT, DNN.

DOI: https://doi.org/10.52254/1857-0070.2025.3-67.16
UDC:621.313

Controler unificat al fluxului de putere pentru sisteme fotoelectrice care utilizează IA pentru a îmbunătăți calitatea energiei electrice folosind un convertor dublu elevator cu inductor conectat

[1]Cindam A., [1]IlanjiAkilandam C., [2]DugyalaV.
[1]Universitatea Annamalai, Cidambaram, India
[2]Institutul de Tehnologie și Știință Kamala, Telangana, India.

Rezumat. Stabilitatea tensiunii, reglarea fluxului de putere și calitatea energiei electrice au devenit probleme majore ca urmare a integrării tot mai mari a surselor de energie regenerabilă, în special a sistemelor fotovoltaice (PV), în rețelele de transport al energiei electrice. Obiectivul principal al acestei cercetări este de a îmbunătăți calitatea energiei electrice (PQ) în sistemul energetic care utilizează Surse de Energie Regenerabilă (RES), în special prin eliminarea conținutului armonic de tensiune și curent care apare de la interfețele electronicii de putere. Pentru a aborda acest lucru, se propune un Controler Unificat al Fluxului de Putere (UPFC), care cuprinde atât convertoare serie, cât și convertoare shunt interconectate cu un condensator de curent continuu. În plus, un sistem fotovoltaic (PV) este integrat cu un convertor Coupled Inductor Dual Boost (CIDB) pentru a asigura o alimentare cu energie stabilă și continuă. Pentru a atinge acest obiectiv, se adoptă o rețea neuronală cu funcții de bază radiale optimizate Coyote (COA-RBFNN) bazată pe urmărirea punctului de putere maximă (MPPT) pentru a asigura extragerea eficientă a energiei din sistemul fotovoltaic. În plus, este integrată o tehnică de control bazată pe o rețea neuronală decuplată (DNN) pentru a gestiona eficient UPFC. Cercetarea este modelată și simulată în Matlab. Cele mai importante rezultate ale studiului demonstrează o îmbunătățire semnificativă a calității energiei generate (PQ), chiar și în condiții de sarcină variabile. Mai mult, convertorul se clasează cu o eficiență îmbunătățită de 88%, cu caracteristici de tensiune și curent îmbunătățite. Semnificația rezultatelor constă în capacitatea de a integra energia regenerabilă cu tehnologiile contemporane de control al puterii, garantând în același timp o furnizare de energie fiabilă și de înaltă calitate.

***Cuvinte-cheie*:** calitatea energiei, fotovoltaica, convertor elevator cu inductor cuplat, algotitm de optimizare Coyote, rețea neuronală.

Унифицированный контроллер потока мощности для фотоэлектрических систем с использованием ИИ для повышения качества электроэнергии с использованием двойного повышающего преобразователя со связанным индуктором

[1]Чиндам А., [1]Иланжиакиландам С., [2]Дугыяла В.
[1]Университет Аннамалаи, Чиндамбаран, Индия
[3] Институт технологий и науки Камалы, Телангана, Индия.

Аннотация. Стабильность напряжения, регулирование потока мощности и качество электроэнергии стали основными проблемами в результате растущей интеграции возобновляемых источников энергии, особенно фотоэлектрических (PV) систем, в сети передачи электроэнергии. Основной целью данного исследования является повышение качества электроэнергии (PQ) в энергосистеме, использующей возобновляемые источники энергии (ВИЭ), в частности, путем устранения гармонических составляющих напряжения и тока, возникающих в интерфейсах силовой электроники. Для решения этой проблемы предлагается унифицированный контроллер потока мощности (UPFC), включающий как последовательные, так и шунтирующие преобразователи, соединенные с конденсатором звена постоянного тока. Кроме того, фотоэлектрическая (PV) система интегрирована с преобразователем со связанными индукторами с двойным повышающим преобразователем (CIDB) для обеспечения стабильной и непрерывной подачи энергии. Для достижения этих целей используется отслеживание точки максимальной мощности (MPPT) на основе оптимизированной радиальной базисной функции нейронной сети Coyote (COA-RBFNN) для обеспечения эффективного извлечения энергии из фотоэлектрической системы. Кроме того, интегрирован метод управления на основе развязанной нейронной сети (DNN) для эффективного управления UPFC. Исследование смоделировано и смоделировано в среде Matlab. Наиболее важные результаты исследования демонстрируют значительное улучшение качества электроэнергии даже при изменении нагрузки. Более того, преобразователь имеет повышенный КПД на 88% и улучшенные характеристики напряжения и тока. Значимость результатов заключается в возможности интеграции возобновляемой энергии с современными технологиями управления электропитанием, гарантируя при этом надежную и высококачественную подачу электроэнергии.

***Ключевые слова*:** качество мощности, фотовольтаика, двойной повышающий преобразователь со связанными индукторами, оптимизированный для Coyote RBFNN MPPT, DNN.

INTRODUCTION

At present, major aim is to attain enhanced alternative for fossil fuel base energy sources due to their hazardous and negative impacts on the environment, which in turn causes severe damages [1]. This issue led to the development of RES based power generation approaches, currently there are various RES available, among which, PV is widely utilized due to simple and easy integration with reduced expenses [2]. However, connecting PV source to the grid produces certain drawbacks including power imbalance and quality issues, which are raised due to the increased harmonics within the PV system. [3] Therefore, considering these shortcomings and to mitigate these limitations, Flexible Alternating Current Transmission Systems (FACTS) are developed [4]. The implementation of FACTS allows smooth connection and transmission of power between the source and receiver [5-6]. Generally, FACTS are connected in series and shunt connections, of which series FACTS devices enable the optimum system performance by balancing the voltage levels, altering active power and allowing improved control of transmission. Series devices include Thyristor Controller Series Capacitor (TCSC) [7], Static Synchronous Series Compensator (SSSC) [8], and Dynamic Voltage Restorer (DVR) [9]. Shunt FACTS devices comprise of various types which includes Static VAR Compensators (SVC) [10] and Static Synchronous Compensators (STATCOM) [11]. Additionally, combining series and shunt devices enable to attain the benefits of both devices, for which the highly considered and demanded device is UPFC [12]. Significantly, UPFC allows controlling the load voltage and rectifying source voltage harmonics. Furthermore, it is essential to attain optimum control of UPFC, for which various control approaches are developed including Adaptive Neuro-Fuzzy (ANFIS) based UPFC [13] designed for high-voltage transmission applications, the implementation of ANFIS-UPFC significantly reduces active power, overshoot and settling, and provides enhanced control performance. However, this approach is prone to increased computational complexity leading to less effective system performance. Consecutively, Artificial Neural Network (ANN) [14] controlled UPFC achieves rapid response rate, enhanced adaptability, increased robustness and higher transmission. But ANN-UPFC requires additional training, which leads to overfitting issues, thereby, increasing the complexity. Henceforth, considering these limitations and to prevail over

them, this paper utilizes DNN for attaining UPFC performance by contributing enhanced ability to adapt towards varying active and reactive power requirements, thus enhancing the entire system stability and reliability. Moreover, to provide consistent and sustainable power supply, PV system is integrated, for which, the initial PV output voltage produced is generally low, which makes it essential for power converters to boost the PV power production [15]. To further extract maximum power along with continuous monitoring, MPPT approaches are preferred. Table 1 displays the merits and demerits of both conventional converters and MPPT approaches.

Table1

Merits and Demerits of both conventional converters and MPPT approaches

Reference	Converter	MPPT	Merits	Demerits
[16]	DC-DC Converter	Ant Bee Colony (ABC)	♦Increased Efficiency ♦Enhanced tracking ability	♦Increased Expenses ♦Computational Complexity
[17]	High Gain DC-DC converter	Adaptive Step Genetic Algorithm (ASGAO) optimized RBFN	♦Increased Voltage gain ♦Reduced Losses	♦Complicated Implementation ♦Increased Processing time
[18]	Interleaved Boost Converter	Adaptive Stepped Scaled Perturb and Observe (ASSPO) optimized ANN	♦Improved System performance ♦Reduced Voltage ripples	♦Requires additional tuning ♦Increased Complexity
[19]	DC-AC Converter	Cuckoo Search Optimized ANN	♦Increased Efficiency ♦Enhanced tracking quality	♦Reduced convergence ♦Increased component count

The integration of PV systems into power grids introduces power quality issues, mainly due to harmonics from power electronic interfaces. FACTS devices offer limited compensation, while UPFC provides a more complete solution but relies heavily on effective control. Conventional control methods face challenges like complexity, slow response, and poor adaptability. Similarly, existing MPPT techniques and converter designs, though efficient, are often complex and lack robustness under variable conditions. These gaps underline the need for an intelligent, integrated framework for efficient energy extraction, resilient UPFC control, and enhanced harmonic mitigation.Considering the demerits of above mentioned conventional converters and MPPT approaches, this paper develops a novel converter and MPPT topology to prevail over the above listed shortcomings. Here, Coupled Inductor Dual Boost converter is deployed along with Coyote optimized RBFNN MPPT approach as in Figure 1. The proposed system is designed and developed using DNN controlled UPFC system which is powered utilizing PV.

PROPOSED SYSTEM MODELLING.

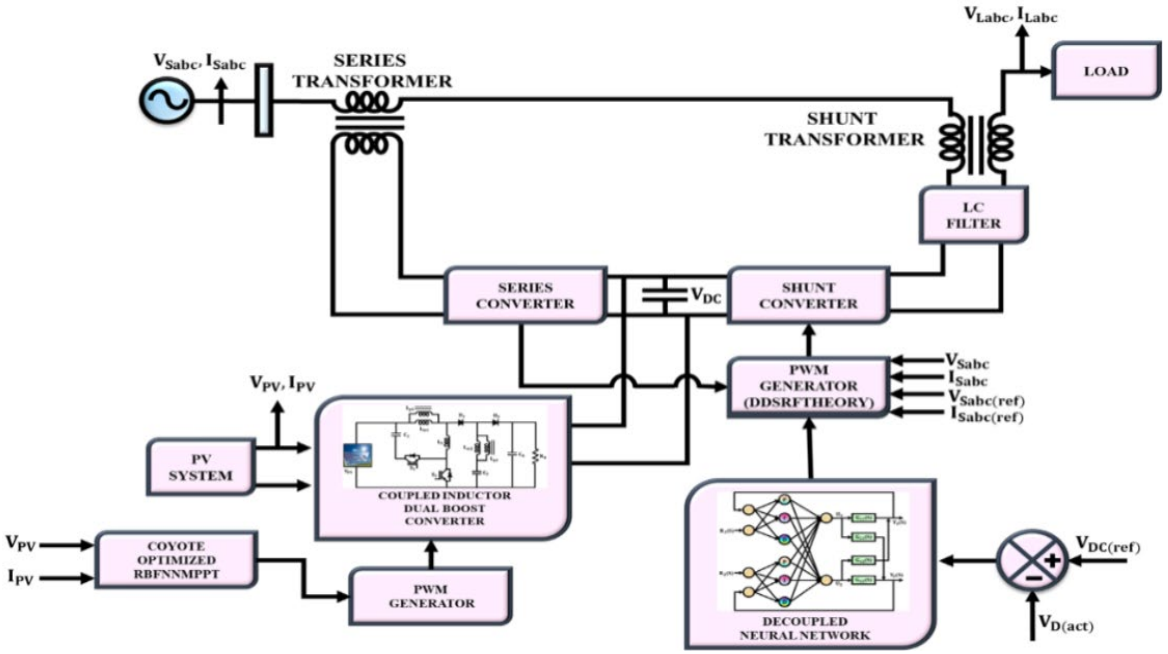

Fig.1. Proposed System Block Diagram.

A.*Modelling of UPFC*

UPFC comprises of both series and shunt active power filters which is illustrated in Figure 2.

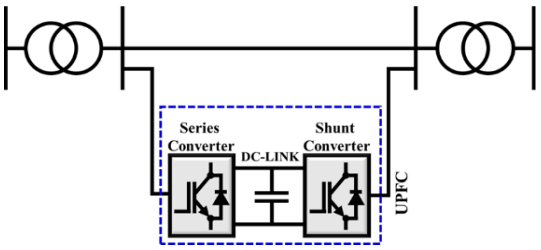

Fig.2. UPFC structure.

a.*Series Converter*

Figure 3 represents the structure of series converter control, here, the voltage is estimated by Phase-Locked Loop (PLL) and then it is transformed into $d-q$ axes via the dq transformer, which is expressed using, Where, V^q indicates the quadrature axes voltage, the three-phase voltages are denoted as $\left[V^a\, V^b\, V^c\right]$ and V^d implies to the direct axes voltage, that is levelled using the low-pass filter, which is attained using,

$$\begin{bmatrix} V^0 \\ V^d \\ V^q \end{bmatrix} = \frac{2}{3}\begin{bmatrix} \frac{1}{2} & \frac{1}{2} & \frac{1}{2} \\ \sin(\alpha t) & \sin(\alpha t-\frac{2\pi}{3}) & \sin(\alpha t+\frac{2\pi}{3}) \\ \cos(\alpha t) & \cos(\alpha t-\frac{2\pi}{3}) & \cos(\alpha t+\frac{2\pi}{3}) \end{bmatrix}\begin{bmatrix} V^a \\ V^b \\ V^c \end{bmatrix} \quad (1)$$

$$V^{d(dc)} = V^d - V^{d(ac)} \quad (2)$$

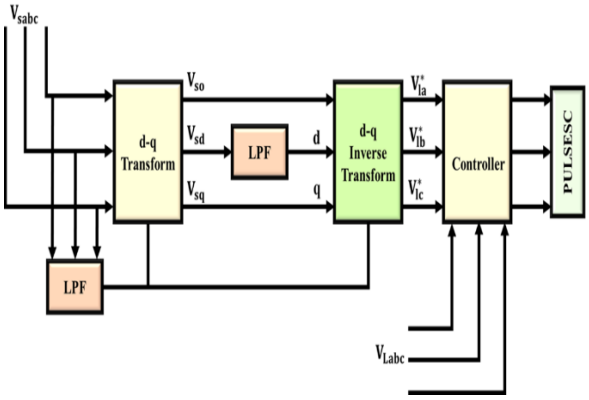

Fig.3.Structure of series converter control.

The dq voltage is then retreated back to the three-phase voltage which is utilized as the reference voltage. Later, the deployed controller compensates the variations attained between these signals.

$$\begin{bmatrix} V^{Ra} \\ V^{Rb} \\ V^{Rc} \end{bmatrix} = \frac{2}{3}\begin{bmatrix} \sin(\alpha t) & \frac{1}{2} & 1 \\ \sin(\alpha t) & \sin(\alpha t - \frac{2\pi}{3}) & 1 \\ \cos(\alpha t) & \cos(\alpha t - \frac{2\pi}{3}) & 1 \end{bmatrix}\begin{bmatrix} V^{d(dc)} \\ V^{q} \\ V^{o} \end{bmatrix} \quad (3)$$

b.Shunt Converter

Figure 4 displays the structure of shunt converter control, where the converter operation starts by transforming current and voltage to $\propto, \beta$ as expressed in equation (4), using which the active and reactive power are calculated by equation (5),

$$\begin{bmatrix} I^{0} \\ I^{\alpha} \\ I^{\beta} \end{bmatrix} = \sqrt{\frac{2}{3}}\begin{bmatrix} \frac{1}{\sqrt{2}} & \frac{1}{\sqrt{2}} & \frac{1}{\sqrt{2}} \\ 1 & \frac{-1}{2} & \frac{-1}{2} \\ 0 & \frac{\sqrt{3}}{2} & -\frac{\sqrt{3}}{2} \end{bmatrix}\begin{bmatrix} I^{a} \\ I^{b} \\ I^{c} \end{bmatrix} \quad (4)$$

$$\begin{bmatrix} P \\ Q \end{bmatrix} = \begin{bmatrix} V^{s\alpha} & V^{S\beta} \\ -V^{S\beta} & V^{s\alpha} \end{bmatrix}\begin{bmatrix} I^{\alpha} \\ I^{\beta} \end{bmatrix} \quad (5)$$

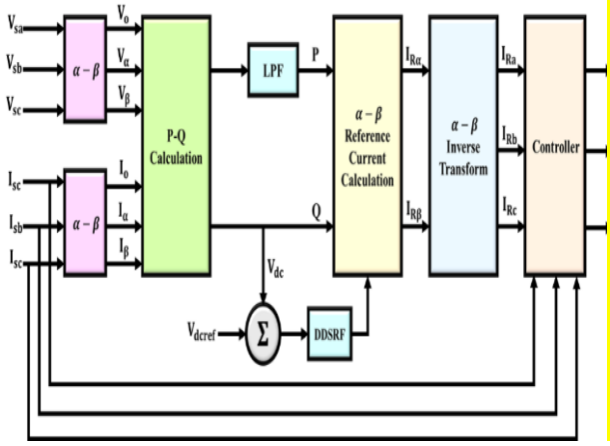

Fig.4. Structure of shunt converter control.

To obtain the reference values for $\propto$ andβ, active power (P) is passed through LPF which is then transformed as represented in equation (6).

$$\begin{bmatrix} I^{Ra} \\ I^{Rb} \\ I^{Rc} \end{bmatrix} = \sqrt{\frac{2}{3}}\begin{bmatrix} 1 & 0 \\ \frac{-1}{2} & \frac{\sqrt{3}}{2} \\ \frac{-1}{2} & -\frac{\sqrt{3}}{2} \end{bmatrix}\begin{bmatrix} I^{R\alpha} \\ I^{R\beta} \end{bmatrix} \quad (6)$$

Moreover, to obtain enhanced UPFC performance by improving its ability to control power flow by enabling to adapt towards varying active and reactive power requirements, DNN using which improves the overall system stability and reliability.

B.*Modelling of DNN*

The DNN based UPFC control approach is utilized to attain enhanced and controlled UPFC performance which is generally multi-layered feed-forward NN structure. Generally, DNN comprises of three layers which is input, hidden and output layer respectively. Figure 5 represents the structure of DNN control system for UPFC, each layer is connected through weights. The major aim of DNN is to attain enhanced control of the system parameters including active and reactive power along with voltage.

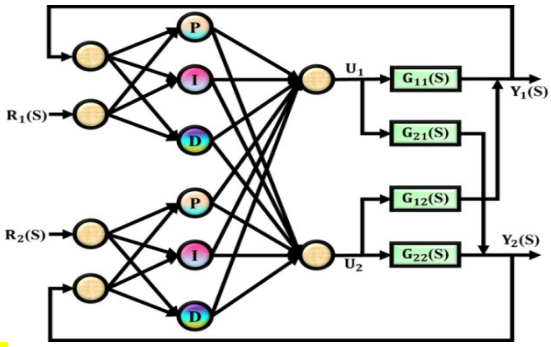

Fig.5. DNN based UPFC control approach.

Here, the input layer is fed with the desired voltage, active and reactive power output values, and hidden layer is where the actual process takes place using the neuron layers which enables control of voltage, active and reactive power. Hidden layer is the composition of PID control structure which are contained as neurons. The PID control structure adjusts the weights via the back-propagation learning algorithm, thereby, attaining decoupling. Lastly, the output layer generates the control signals including the series voltage and shunt reactive power. Furthermore, the to assure accurate control signals for both series and shunt converter, DDSRF theory based PWM generator is deployed which enables increased robustness for grid-connected PV based UPFC system.

C.M*odelling of DDSRF Theory based PWM Generator*

The DDSRF, three phase power component is determined using,

$$\begin{bmatrix} V_{as} \\ V_{bs} \\ V_{cs} \end{bmatrix} = V_0 \begin{bmatrix} y(\omega t+\varphi_1) \\ y(\omega t-\frac{2\pi}{3}+\varphi_1) \\ y(\omega t+\frac{2\pi}{3}+\varphi_1) \end{bmatrix} + V_2 \begin{bmatrix} y(\omega t+\varphi_2) \\ y(\omega t-\frac{2\pi}{3}+\varphi_2) \\ y(\omega t+\frac{2\pi}{3}+\varphi_2) \end{bmatrix} (7)$$

The unsymmetrical voltage source is expressed using,

$$V_S = \begin{bmatrix} V_{as} \\ V_{bs} \\ V_{cs} \end{bmatrix} = \begin{bmatrix} V_{ao} \\ V_{bo} \\ V_{co} \end{bmatrix} + \begin{bmatrix} V_{a1} \\ V_{b1} \\ V_{c1} \end{bmatrix} + \begin{bmatrix} V_{a2} \\ V_{b2} \\ V_{c2} \end{bmatrix} \quad (8)$$

And the current source component is,

$$I_S = \begin{bmatrix} I_{as} \\ I_{bs} \\ I_{cs} \end{bmatrix} = \begin{bmatrix} I_{ao} \\ I_{bo} \\ I_{co} \end{bmatrix} + \begin{bmatrix} I_{a1} \\ I_{b1} \\ I_{c1} \end{bmatrix} + \begin{bmatrix} I_{a2} \\ I_{b2} \\ I_{c2} \end{bmatrix} \quad (9)$$

According to Clark's transformation, three-phase voltage is determined as,

$$V_{\alpha\beta 0} = \frac{2}{3} \begin{bmatrix} 1 & -\frac{1}{2} & -\frac{1}{2} \\ 1 & \frac{\sqrt{3}}{2} & \frac{\sqrt{3}}{2} \\ 0 & \frac{1}{2} & \frac{1}{2} \end{bmatrix} V_S \quad (10)$$

Significantly, the real and imaginary power is calculated utilizing,

$$\begin{bmatrix} p \\ q \end{bmatrix} = \begin{bmatrix} V_\alpha & V_B \\ -V_B & V_\alpha \end{bmatrix} \quad (11)$$

Considering the stationary reference frame, the voltage vector comprises of similar frequency as of the rotating system angular frequency. Thus, by dividing the positive and the negative sequence component, the Park's transformation equation is determined using,

$$V_{dq1} = V_{\alpha\beta} \begin{bmatrix} \cos(\omega t) & -\sin\omega t) \\ -\sin\omega t) & \cos(\omega t) \end{bmatrix} (12)$$

$$V_{dq2} = V_{\alpha\beta} \begin{bmatrix} -\cos(\omega t) & -\sin\omega t) \\ \sin\omega t) & -\cos(\omega t) \end{bmatrix} \quad (13)$$

Based on the above equations,

$$V_{dq1} = -V_{dq2} \quad (14)$$

Significantly, the instantaneous PQ theory obtained from Park's transformation is attained using the decoupled current and voltage values,

Which are calculated using,

$$P_1 = \frac{3}{2}\begin{bmatrix} V_{d1} - V_{d2} V_{q2} \end{bmatrix} \begin{bmatrix} I_{q2} \\ I_{d2} \\ I_{q1} \\ I_{d1} \end{bmatrix} \quad (15)$$

$$Q_1 = P_2 = \frac{3}{2}\begin{bmatrix} V_{d1} V_{q1} V_{d2} V_{q2} \end{bmatrix} \begin{bmatrix} I_{q2} \\ I_{d2} \\ I_{q1} \\ I_{d1} \end{bmatrix} \quad (16)$$

$$Q_2 = \frac{3}{2}\begin{bmatrix} V_{d1} - V_{q1} V_{d2} - V_{q2} \end{bmatrix} \begin{bmatrix} I_{q2} \\ I_{d2} \\ I_{q1} \\ I_{d1} \end{bmatrix} \quad (17)$$

According to the decoupled current and voltage, the reference signal generated is represented as,

$$P_0 = \frac{3}{2}\begin{bmatrix} V_{d1} - V_{q1} - V_{d2} V_{q2} \end{bmatrix} \begin{bmatrix} I_{q2} \\ I_{d2} \\ I_{q1} \\ I_{d1} \end{bmatrix} \quad (18)$$

$$Q_0 = P_2 = \frac{3}{2}\begin{bmatrix} V_{d1} V_{q1} V_{d2} V_{q2} \end{bmatrix} \begin{bmatrix} I_{q2} \\ I_{d2} \\ I_{q1} \\ I_{d1} \end{bmatrix} \quad (19)$$

Henceforth, the reference voltage and current for compensating the source voltage deviations and the load current harmonics is obtained through DDSRF Theory based PWM generator.

E.*Modelling of PV fed Coupled Inductor Dual Boost converter*

Coupled Inductor Dual Boost converter in Figure 6 operates in four different modes which are given in Figure 7. Figure 8 represents the timing diagram of the proposed converter attained during the operating modes.

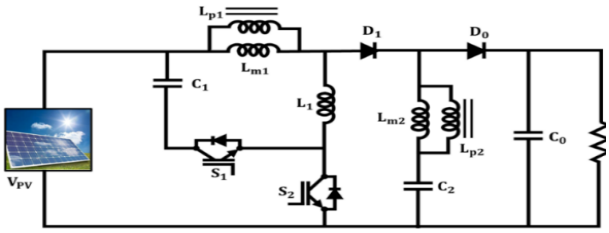

Fig.6. Coupled Inductor Dual Boost Converter.

Mode 1:

In this mode, both the switches S_1 and S_2 are kept in ON condition, thus both the coupled inductors CI_1 and CI_2 provide energy to the output, while the output diode current keeps decreasing until it becomes zero.

$$v_x = \frac{2nv_{in} + v_0}{2n+1} \tag{20}$$

$$v_{Lm_1} = \frac{v_{in} - v_0}{2n+1} \tag{21}$$

$$v_{Lm2} = \frac{-(v_{in} - v_0)}{2n+1} \tag{22}$$

And the magnetizing inductor current, resonant current and diode current is given by,

$$i_{Lm_1}(t) = \frac{v_{in} - v_0}{(2n+1)L_m}(t) + i_{Lm_1}(t_1) \tag{23}$$

$$i_{Lm_2}(t) = \frac{-(v_{in} - v_0)}{(2n+1)L_m}(t) + i_{Lm2}(t_1) \tag{24}$$

$$i_{Lr}(t) = \frac{2nv_{in} + v_0}{(2n+1)L_r}(t) + i_{Lr}(t_1) \tag{25}$$

$$i_{DO(t)} = \frac{i_{Lm1}(t) - i_{Lm2}(t) - i_{Lr}(t)}{2n+1} \tag{26}$$

Mode 2:

Switch S_1 is turned ON and switch S_2 is turned OFF, here, switch S_1 enable to store energy in magnetizing inductor. And the output power is supplied through the capacitor discharge respectively

Mode 3:

In mode 3, S_2 is OFF, while S_1 is kept in ON state, where as diode D_0 is also turned OFF, leading to direct delivery of input voltage to the inductor and the magnetizing inductor. Moreover, the load is charged through the discharging of capacitor C_0 respectively.

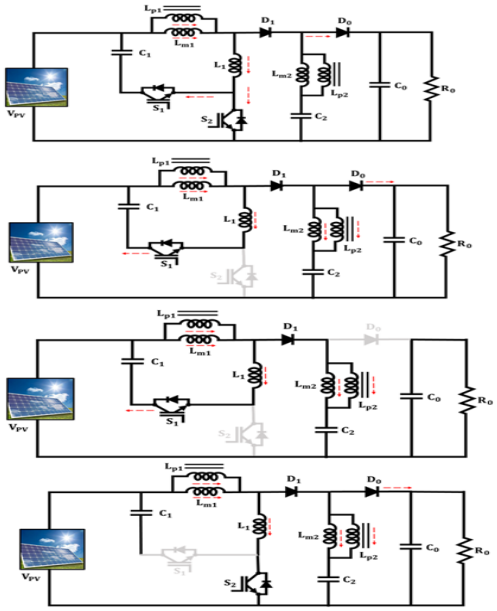

Fig.7.Modes of operation.

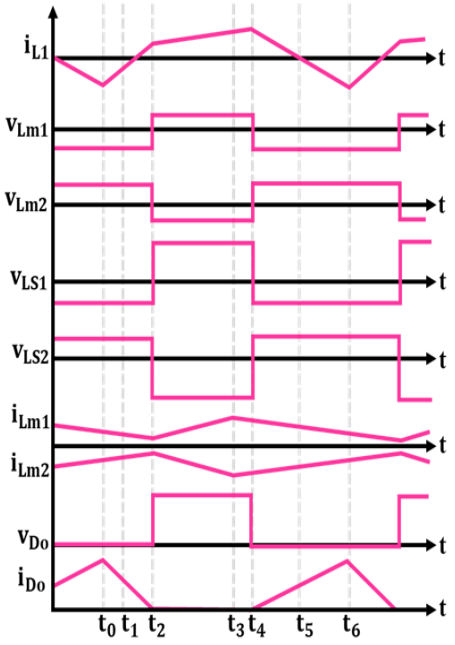

Fig. 8. Timing Waveform proposed converter.

Mode 4:

During this mode, switch S_1 is kept in OFF state, while S_2 is ON. Here, S_1 is kept in OFF state making v_{Lm1} quite similar to the input voltage and v_{Lm2} similar to the negative input voltage and the output current is delivered via the capacitor C_0 respectively.

$$v_X = V_{IN}\frac{2 \cdot L_R}{L_M + 2L_R}. \tag{27}$$

$$v_{Lm1} = V_{IN}\frac{2\cdot L_R}{L_M + 2L_R} \quad (28)$$

$$v_X = -V_{IN}\frac{2\cdot L_R}{L_M + 2L_R}. \quad (29)$$

F.*Modelling of Coyote Optimized RBFNN based MPPT*

Figure 9 showcases the representation of RBFNN.

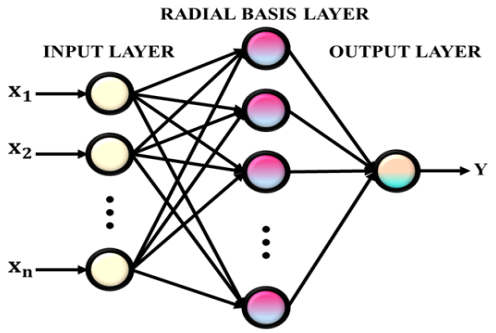

Fig. 9. RBFNN architecture.

The relation among the hidden and output layer is depicted by,

$$h_j = e^{-\|x-c_j\|^2/2\sigma_j^2} \quad (30)$$

$$y_k = \sum_{j=1}^{h} w_j, kh_j \quad (31)$$

Where, d, h and o indicates the number of neurons present in the input, hidden and output layer respectively. x_i, h_j and y_k indicates the i_{th}neuron in the input layer, j_{th} neuron in the hidden layer $v_X = V_{IN}\frac{2\cdot L_R}{L_M + 2L_R}$ and the k_{th} neuron in the output layer. The input vectors name $i_{sx} = \left[x_1,\ x_2, \ldots,\ x_d\right]^T$. $W_{j,k}$ represents the output weights. The j_{th} neuron centre vector is denoted byc_j, σ_j indicates the width of the hidden neuron and$\|x - c_j\|$denotes the Euclidean distance among the input and the output vector. To further enhance RBFNN performance, tuning algorithm plays a major part, by deploying these algorithms enables to attain enhanced tuning of RBFNN parameters. Here, RBFNN parameters are tuned using the Coyote Optimization algorithm. COA is preferred over other optimization techniques due to its balanced exploration and exploitation capabilities, inspired by the intelligent and adaptive social behavior of coyotes in nature. Unlike traditional algorithms, which may suffer from premature convergence or require extensive parameter tuning, COA dynamically adapts to the search environment, maintaining diversity in the population and avoiding local optima traps. Its lightweight structure, minimal control parameters and high convergence speed make it especially suitable for real-time applications. Additionally, COA exhibits robust performance across a wide range of nonlinear, multidimensional optimization problems, providing a more reliable and computationally efficient solution compared to other heuristic approaches. The flow chart is presented in Figure 10. The integration of COA enables to attain improved convergence speed, robustness and reliability by providing accurate tracking of MPP even under varying environmental circumstances. COA is a population-based algorithm that is developed replicating the behaviour of coyotes. Where, in COA, the total populations of the coyotes are divided into N_P *and* N_C .Therefore, the entire population of COA is attained by multiplying N_p andN_c. Where, for each coyote in the pack at time particular instinct is represented using, $x = \left(x_1,\ x_2,\ \ldots,\ x_j\right) = soc_c^{p,I}$ where, j indicates the dimension of the search space respectively.

The COA operation starts with initializing the global population of the coyotes, that is for each coyote in the pack comprising of j_{th} dimension is given by,

$$soc_c^{p,1} = lb_j + r_j(ub_j - lb_j),\ \ j = 1,2,\ldots\ldots,j \quad (32)$$

Where, lb_j and ub_j indicates the lower, upper bound, r_j represents the randomly generated real number ranging between 0 and 1 respectively.

The second step is to determine the present social condition, which indicates the objective function cost,

$$fit_c^{p,t} = f(soc_c^{p,t}) \quad (33)$$

$$P_e = 0.005N_C^2 \quad (34)$$

Considering equation (36), to prevent from P_e becoming greater than 1, N_c is restricted to certain limit, then the updated coyote social condition is expressed using,

$$new_{soc_c^{p,t}} = soc_c^{p,t} + r_1\delta_2 + r_2\delta_2 \quad (35)$$

Where, r_1 and r_2 indicates the equally divided random numbers between 0 and 1 respectively. Here, δ_1 and δ_2 is given by,

$$\delta_1 = \alpha^{p,t} - soc_{cr_1}^{p,t} \quad (36)$$

$$\delta_2 = \beta^{p,t} - soc_{cr2}^{p,t} \quad (37)$$

Where,

$$\beta_j^{p,t} = \begin{cases} s_{(N_c+1)/2\,j}^{p,t} & N_c \text{ is odd} \\ \dfrac{s_{N_c/2\,j}^{p,t} + s_{N_c+1/2\,j}^{p,t}}{2}, & otherwise \end{cases} \quad (38)$$

$$\alpha^{p,t} = \left\{ socI_{c\varepsilon C^{\min f(soc_c^{p,t},)}}, c = \{1,2,....N_C\} \right\}$$

The new social condition is calculated using,

$$new_{fit_c^{p,t}} = f\left(new_{soc_c^{p,t}}\right) \quad (39)$$

It is determined utilizing,

$$soc_c^{p,\,t+1} = \begin{cases} new_{soc_c^{p,t}}, & new_{file_c^{p,t}} < fit_c^{p,t} \\ soc_c^{p,t}, & otherwise \end{cases} \quad (40)$$

The birth of the new coyote is represented using,

$$pup_j^{p,t} = \begin{cases} soc_{k_1,j}^{p,t}, & rnd_j < p_s \text{ or } j = j_1 \\ soc_{k_2,j}^{p,t}, & rnd_j < p_s + p_a \text{ or } j = j_2 \\ R_j, & otherwise \end{cases} \quad (41)$$

Where, $p_s = 1/j$, $p_a = (1-p_s)/2,$, here k_1 and k_2 are the randomly chosen coyotes from $p-th$ pack, j_1 and j_2 are random dimensions, p_s indicates scatter property, p_a denotes association property, R_j implies the random number and finally rnd_j is random number between 0 and 1 respectively.Therefore, the overall proposed system ensures improved system control performance by achieving stable and reliable power supply with enhanced output power quality even under varying system circumstances.

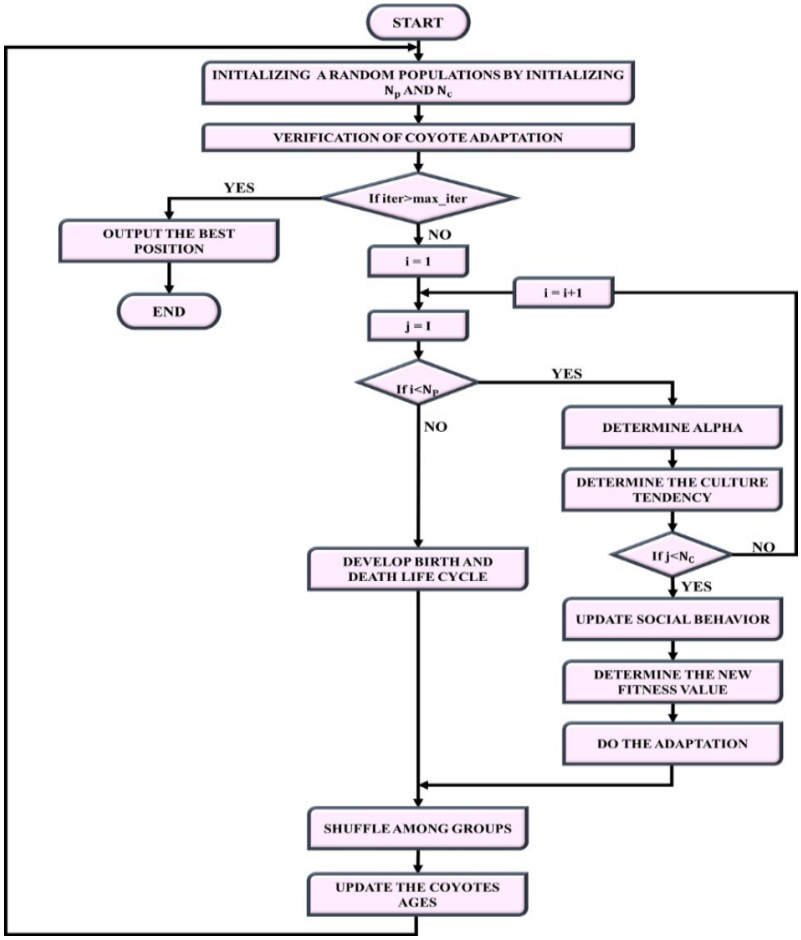

Fig. 10. COA optimized Flowchart.

RESULTS AND DISCUSSION

The developed UPFC system powered using PV with novel converter and MPPT approach is implemented using MAT lab with specifications in Table 2 and their obtained results are discussed in detail along with their comparative analysis in this section.

Table 2

Parameter Specifications

Parameters	Values
PV system	
Open circuit voltage	37.25V
V_{in}	29.95V
I_m	8.35 Amps
Connected in series	2
Short Circuit Voltage	8.95A
Connected in Parallel	7

CI-Dual Boost Converter	
Switching Frequency	10 kHz
$L_{p1}, L_{m1}, L_1, L_{p2}, L_{m2}$	4.7 mH
C_1, C_2	22 µF

The simulations are carried out at sag and swell conditions for testing real-time adaptability. PV source acts as the main energy input and the DC-link capacitor couples series and shunt converters. The DC-link reference voltage is set around 600-750V, the capacitor voltage and inductor current are initially assumed to be zero.

SAG CONDITION

In Figure 11, the occurrence of sag condition is clearly illustrated along with PF waveform.

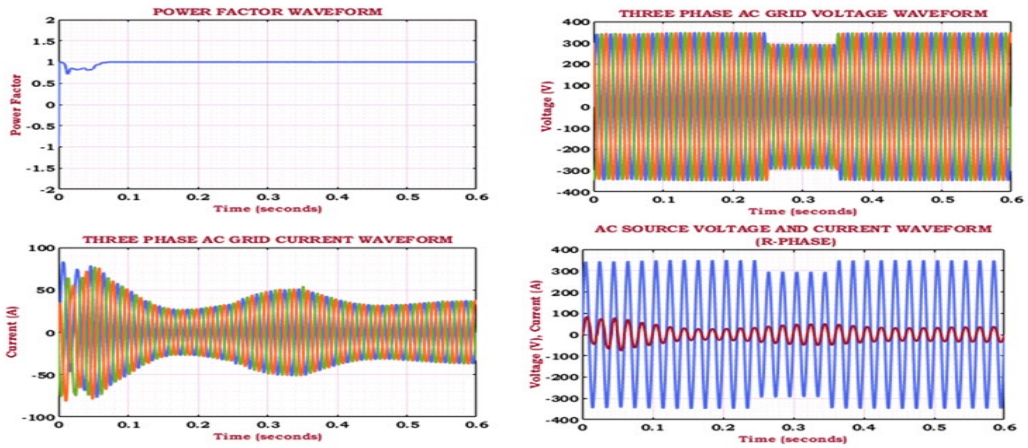

Fig.11. Power Factor and Three Phase AC grid Performance waveform.

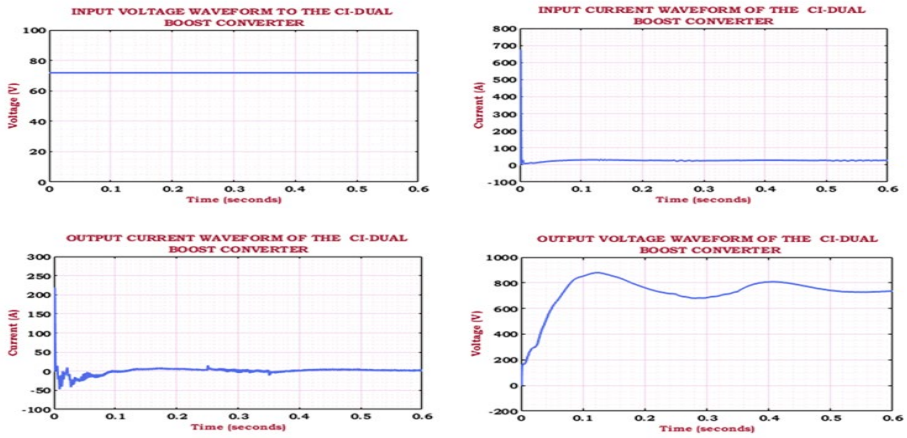

Fig.12. Input and output waveform of CI-dual Boost converter.

Figure 12 represents the CI-dual Boost converter performance, where the first graph showcases the input voltage waveform of the proposed converter which depicts stable and consistent value of around 70 V without any fluctuations for the entire taken time period of 0.6 seconds. While, the second graph implies the input current, which immediately drops down and further shows minor deviations. Significantly, the output current and voltage waveform are provided, in which the both the current and voltage shows major fluctuations. Figure 13 indicates the DC-Link voltage waveform under sag condition, where it is depict able that, the voltage progressively rises with gradual fluctuations and later continues to fluctuate, indicating the voltage fluctuates due to sag condition which needs to be stabilized for better system performance.

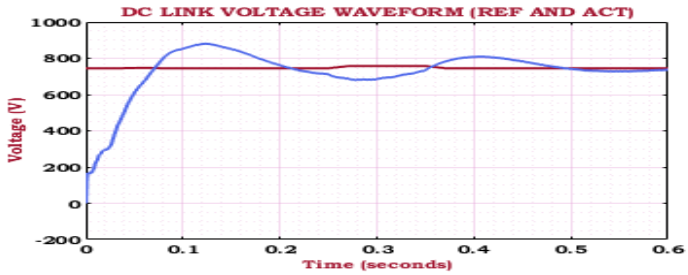

Fig. 13.DC-Link Voltage waveform.

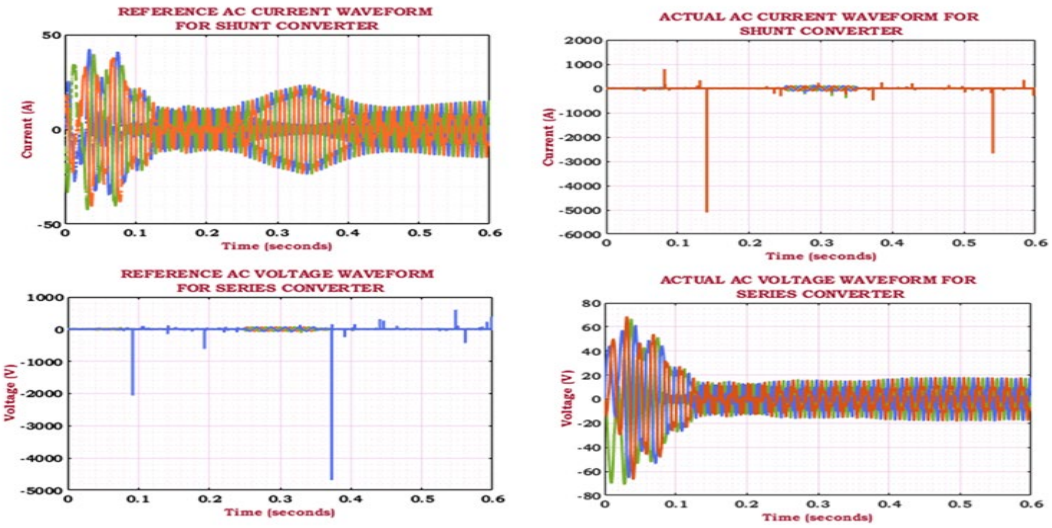

Fig. 14. Reference/Actual AC voltage and current Waveform.

Figure 14 implies the reference/actual AC voltage and current for the series and shunt converter. In Figure 15, the first two graph depicts the three-phase load voltage and current waveform.

.

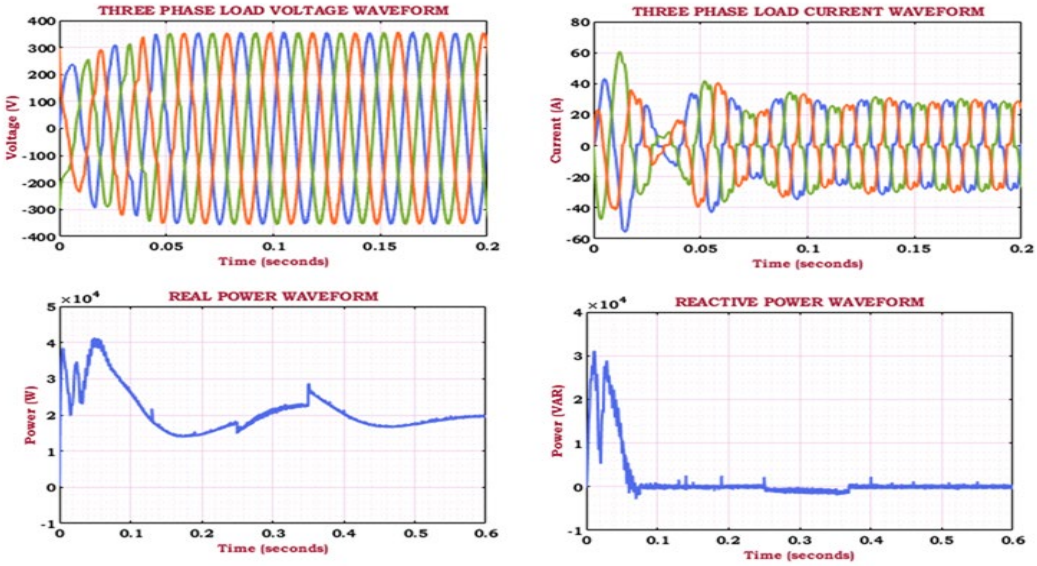

Fig.15. Three Phase Load voltage and current waveform with real and reactive power.

SWELL CONDITION

In Figure 16 below denotes the three-phase AC grid performance waveform along with power factor, where the graph shows that, power factor rapidly increases with certain deviations and later stabilizes at around 0.1 seconds and later is continuously maintained at that value. The second graph comprising the three-phase AC grid voltage is initially maintained between the voltages of ±300V, which then around 0.3 seconds slightly rises and later is maintained at the previous voltage level. Significantly, the third graph depicts the three-phase AC gird current waveform, which shows fluctuations. Finally, the last graph comprises of both three-phase grid voltage and current waveform.

.

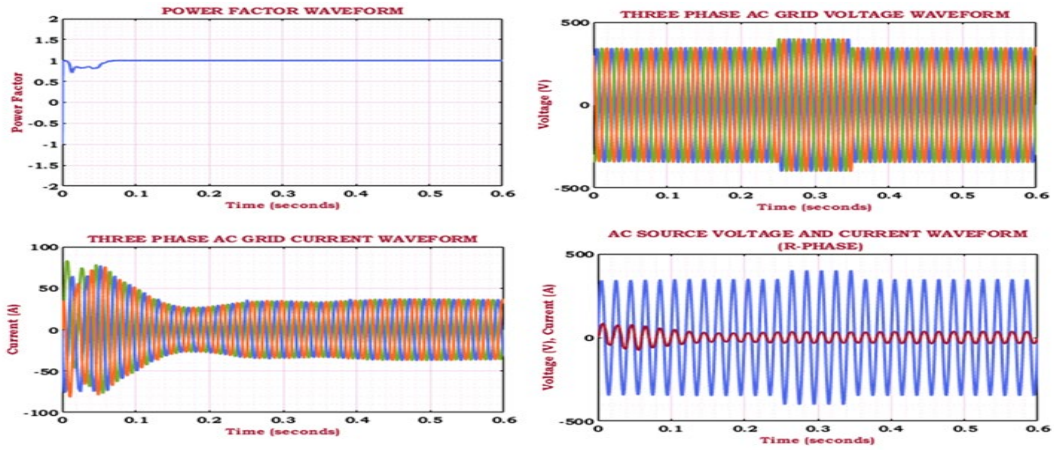

Fig. 16. Three phase grid performance waveform

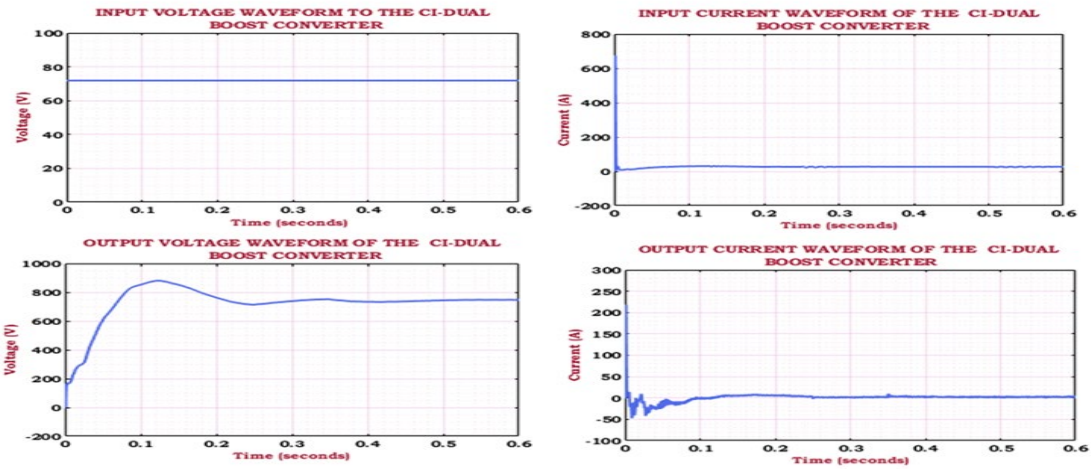

Fig. 17. CI-Dual Boost Converter Performance waveform.

Figure17above indicates the converter input/output voltage and current waveform.

Figure 18 demonstrates the DC-Link voltage waveform

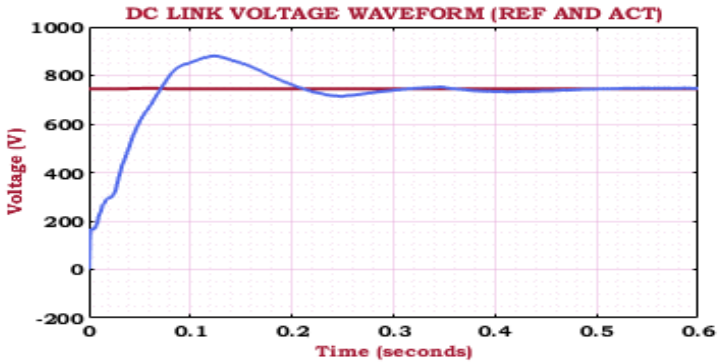

Fig. 18 .DC-Link voltage.

The efficiency of the converter is calculated by,

$$\text{Efficiency } (\eta) = \frac{P_{out}}{P_{in}} \times 100\%$$

$$= \frac{750 \times 0.82}{70 \times 10} \times 100\%$$

$$= 88\%$$

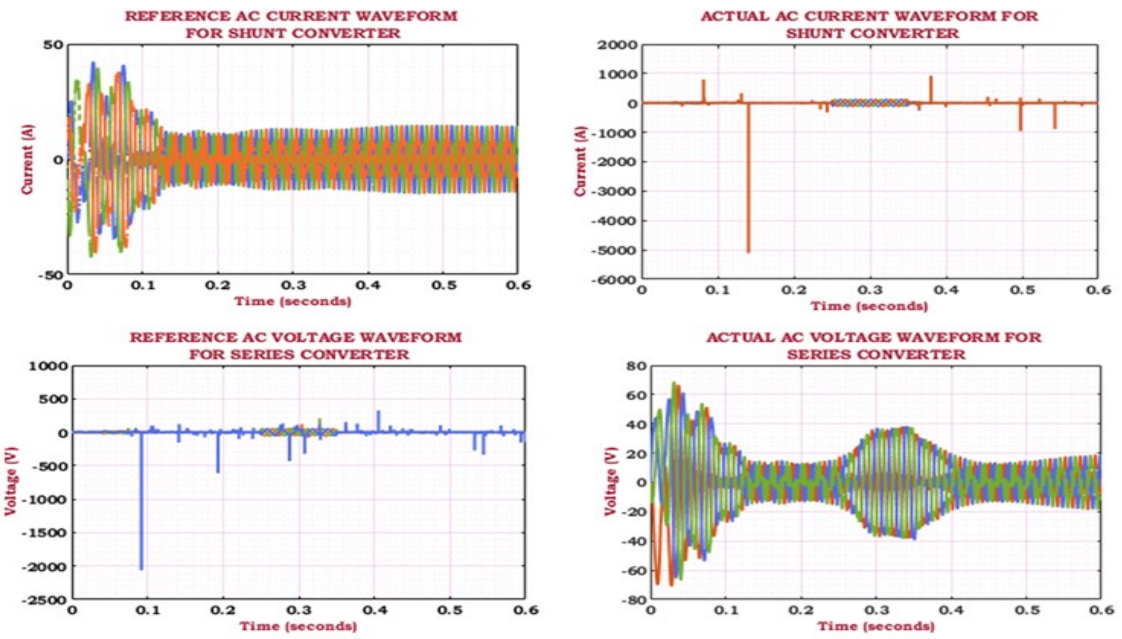

Fig.19. Reference AC voltage and current waveform.

Figure 19 represents the reference/actual current and voltage waveform for both the series and shunt converter. Where the first two graph showcases the reference and actual current waveform for the shunt converter, here both reference and actual current shows certain oscillations and fluctuations. The other two graphs depict the reference and actual voltage for the shunt converter which also contains minor fluctuations.

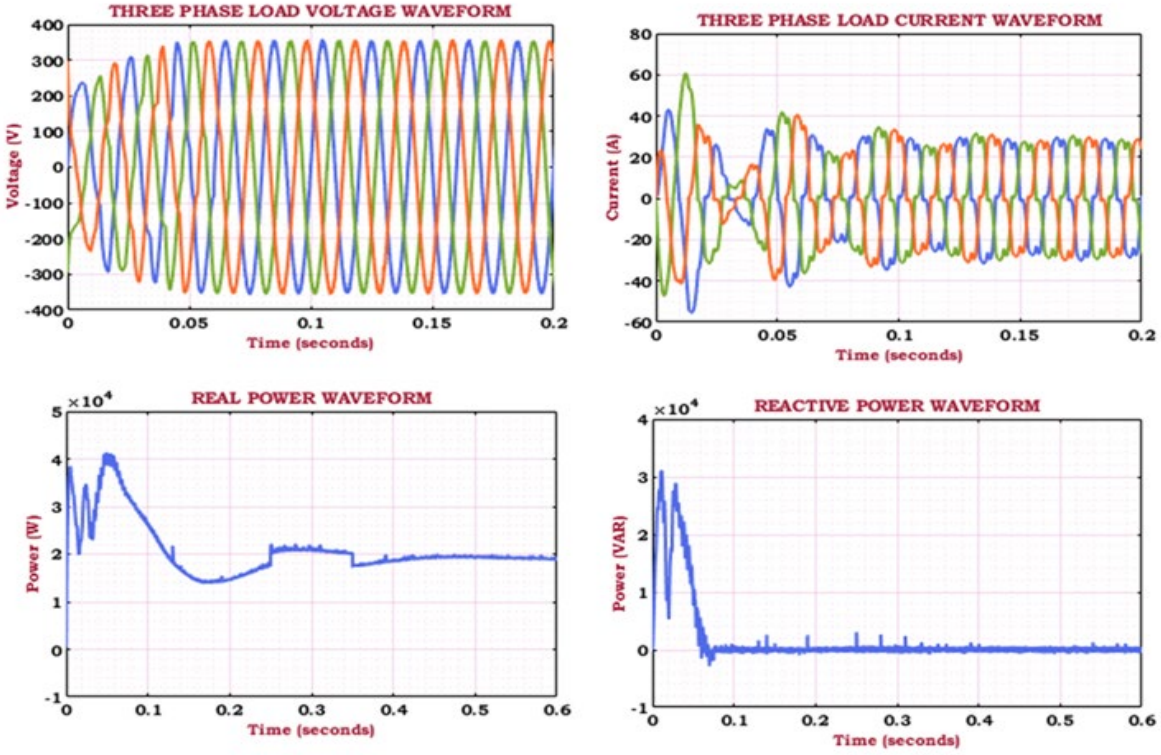

Fig. 20. Three Phase Load performance waveform with Real and Reactive power.

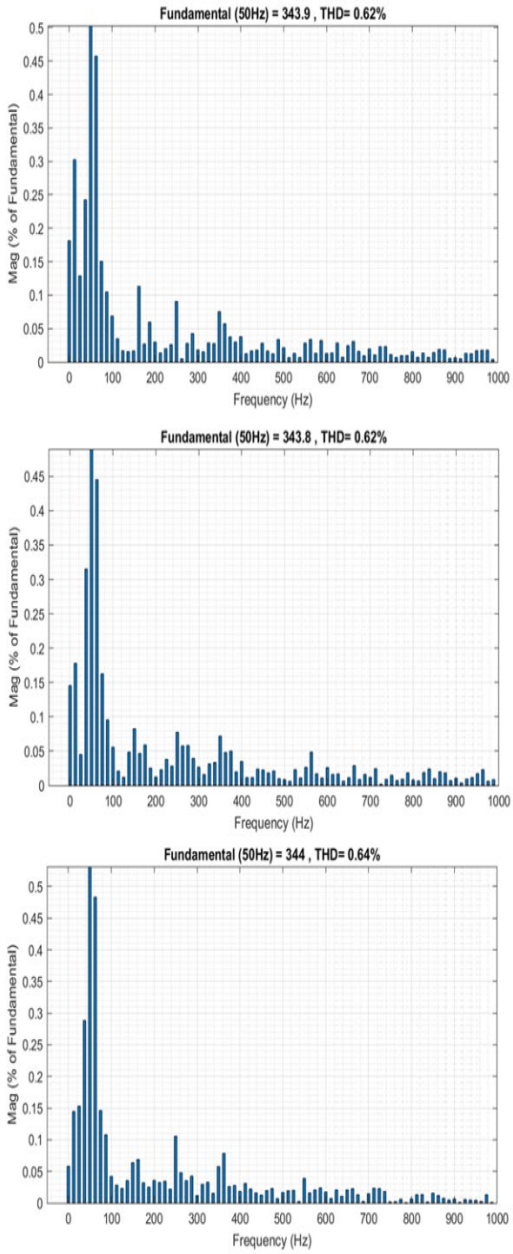

Fig. 21. THD waveforms

Figure 20 indicates the three-phase load voltage and current waveform along with real and reactive power waveform. Figure 21 shows the THD waveforms for three phases A, B, C indicating values of 0.62%, 0.62% and 0.64% respectively. Figure 22 implies the comparison graph between the proposed MPPT approach and other conventional technique like ABC-MPPT [16]. And from the above graph it is evident that proposed MPPT approach depicted improved performance.

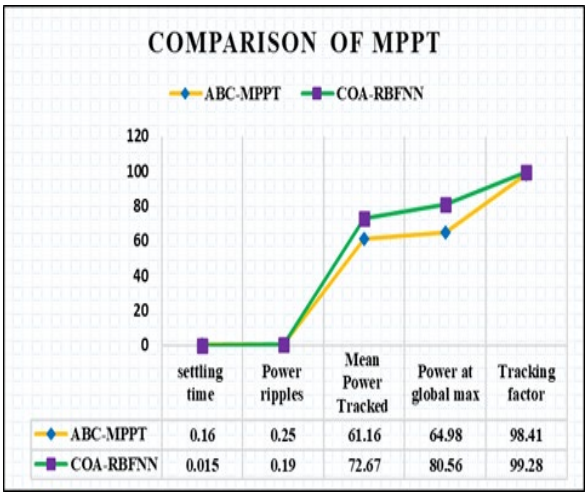

Fig.22. Comparison of MPPT Approach

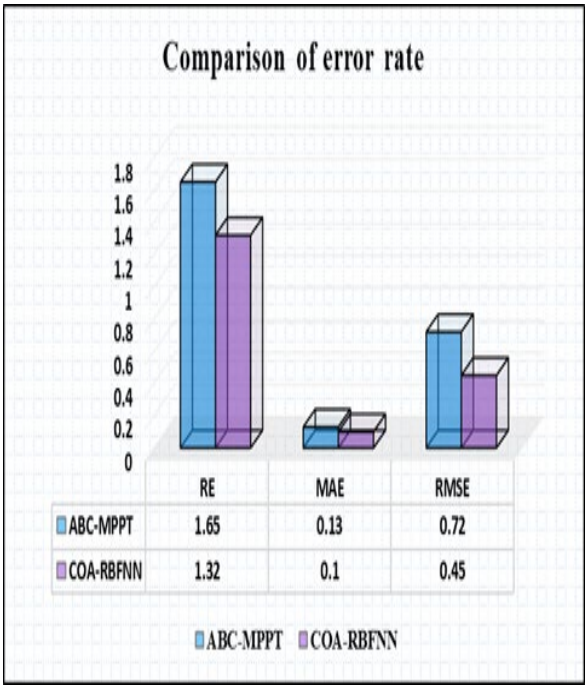

Fig.23.Comparison of error rate

Figure 23 indicates the error rate comparison between the proposed approach and ABC based MPPT [16], where it is notable that, proposed Approach attained comparably reduced error than that of the conventional technique, referring to the highly stable and reliable MPPT performance Table 3 represents the comparison of UPFC control topologies which implies the superior performance of the proposed DNN controlled UPFC than the other approaches.

Table 3

Comparison of UPFC Control topologies

UPFC control Approach	**Receiving End Power**	**Power Loss**	**Loss Minimized**
ANFIS-UPFC [20]	330.5	25	71.50
DNN-UPFC	340	18	85.30

Table 4

THD comparison

Ref	Published Year	Method	Load Voltage THD%			Source Current THD%		
			Phase A	Phase B	Phase C	Phase A	Phase B	Phase C
[21]	2023	SRF, Robust	1.0~1.5%			1.0~1.5%		
[22]	2023	ANFIS, SRF	-	-	-	1.77%	1.77%	1.77%
[23]	2022	ANN	0.72%	0.71%	0.71%	2.97%	2.96%	2.97%
[24]	2022	ANN, SRF	2.3%	1.7%	1.6%	1.3%	1.4%	1.3%
[25]	2022	PI, SRF	2.4%	1.9%	1.6%	2.5%	2.6%	2.4%
Prop	-	COA-RBFNN-DNN	0.59%	0.65%	0.64%	0.62%	0.62%	0.64%

Table 4 presents a comparative analysis of THD. The table highlights various hybrid and intelligent control techniques. Most previous works show moderate THD performance, with voltage THD ranging from 0.71% to 2.4% and current THD from 1.3% to 2.97%. Notably, the proposed COA-RBFNN-DNN approach achieves the lowest THD values, with voltage THD between 0.59% and 0.65% and current THD between 0.62% and 0.64% across all three phases. This indicates superior harmonic suppression capabilities of the proposed method, making it highly effective for power quality enhancement compared to existing techniques.

CONCLUSION

The proposed COA-RBFNN-DNN-based UPFC system demonstrates significant improvement in PQ enhancement by effectively minimizing voltage and current harmonics. The integration of a coupled inductor dual boost converter enables high voltage gain with reduced losses, while the COA-optimized RBFNNbased MPPT achieves faster convergence, lower power ripples and higher tracking accuracy of 99.28% compared to traditional techniques. Moreover, the system exhibits a converter efficiency of 88% and achieves superior harmonic suppression, with voltage THD reduced to as low as 0.59% and current THD to 0.62%, outperforming existing methods. Despite these achievements, the system validation is confined to MATLAB/Simulink simulations, lacking hardware implementation. Future research could explore hardware-in-the-loop (HIL) testing, incorporation of real-time adaptive learning models to further enhance robustness and scalability.

Conflict of interest. The authors declare that they have no conflicts of interest.

References

[1] Osama abed el-Raouf, M., Soad A. A. Mageed, M. M. Salama, Mohamed I. Mosaad, and H. A. AbdelHadi. "Performance enhancement of grid-connected renewable energy systems using UPFC." Energies 16, no. 11 (2023): 4362.

[2] Indukuri, Swetha Monica, Alok Kumar Singh, and D. Vijaya Kumar. "An RFCSO-based grid stability enhancement by integrating solar

photovoltaic systems with multilevel unified power flow controllers." Energy Storage and Saving 3, no. 4 (2024): 341-351.

[3] Senthil Kumar, R., K. MohanaSundaram, and K. S. Tamilselvan. "Hybrid Reference Current Generation Theory for Solar Fed UPFC System." Energies 14, no. 6 (2021): 1527.

[4] Khaleel, Mohamed, ZıyodullaYusupov, Nassar Yasser, HalaElkhozondar, and Abdussalam Ali Ahmed. "An integrated PV farm to the unified power flow controller for electrical power system stability." Int. J. Electr. Eng. and Sustain. (2023): 18-30.

[5] Kavin, K. S., P. SubhaKaruvelam, M. Devesh Raj, and M. Sivasubramanian. "A Novel KSK Converter with Machine Learning MPPT for PV Applications." Electric Power Components and Systems (2024): 1-19.

[6] Sangeetha, P., and L. Shirisha. "POWER QUALITY IMPROVEMENT IN RENEWABLE ENERGY-BASED DISTRIBUTED GENERATION SYSTEMS USING ANFIS-TUNED UPQC." Journal of Southwest Jiaotong University 59, no. 2 (2024): 492-515.

[7] Polishetty, Vinay Kumar, G. Balamurugan, and KartigeyanJayaraman. "Wind Integrated UPFC System with Cascaded Fuzzy Logic Controller for Alleviation of PQ Issues." GMSARN International Journal (2025): 137-151.

[8] Zhang, Ke, Zhijun Chen, Jun Wang, Chao Yu, Haodong Long, and Chuyang Wang. "A Fast-response Power-Flow Control Strategy of MMC-UPFC based on Active Disturbance Rejection Control." IEEE Access (2024).

[9] Thentral, Thamizh, R. Jegatheesan, and C. Subramani. "New PQ theory for power quality improvement using modular multilevel converter based UPFC system." Journal of Intelligent & Fuzzy Systems 40, no. 4 (2021): 7653-7665.

[10] Senapati, Rudranarayan, VamsiramIlla, Sarat Chandra Swain, and Rajendra Narayan Senapati. "Voltage and current profile improvement of a PV-integrated grid system employing sinusoidal current control strategy based unified power quality conditioner." Materials Today: Proceedings 39 (2021): 1866-1875.

[11] Goud, B. Srikanth, Ch Rami Reddy, Mohit Bajaj, Ehab E. Elattar, and Salah Kamel. "Power quality improvement using distributed power flow controller with BWO-based FOPID controller." Sustainability 13, no. 20 (2021): 11194.

[12] Ahmed, Raghad Hameed, and Ahmed Said Nouri. "Improvement of the Power System's Transient Stability Using the Unified Power Flow Controller with Fuzzy Logic Technique." Journal of Techniques 5, no. 3 (2023): 61-72.

[13] Lund, Asif Ali, Muhammad Usman Keerio, Mohsin Ali Koondhar, Muhammad Ismail Jamali, and Abdul QadeerTunio. "Investigation of advanced control for unified power flow controller (UPFC) to improve the performance of power system." Journal of Applied and Emerging Sciences 11, no. 1 (2021): pp-67.

[14] Zand, Mohammad, MortezaAzimiNasab, SanjeevikumarPadmanaban, PandavKiranMaroti, and S. M. Muyeen. "Sensitivity analysis index to determine the optimal location of multi-objective UPFC for improvement of power quality parameters." Energy Reports 10 (2023): 431-438.

[15] Padaki, Rekha G., and HR Sudarshana Reddy. "An innovative Hybridized optimization perspective for optimal allocation of UPFC, FACTS and SVC." Journal of Integrated Science and Technology 12, no. 4 (2024): 796-796.

[16] González-Castaño, Catalina, Carlos Restrepo, Samir Kouro, and Jose Rodriguez. "MPPT algorithm based on artificial bee colony for PV system." Ieee Access 9 (2021): 43121-43133.

[17] Kumar, Sunkara Sunil, and K. Balakrishna. "A new wide input voltage DC-DC converter for solar PV systems with hybrid MPPT controller." Scientific Reports 14, no. 1 (2024): 10639.

[18] Krishnaram, K., T. Suresh Padmanabhan, Faisal Alsaif, and S. Senthilkumar. "Performance optimization of interleaved boost converter with ANN supported adaptable stepped-scaled P&O based MPPT for solar powered applications." Scientific Reports 14, no. 1 (2024): 8115.

[19] Ibrahim, Nagwa F., Mohamed Metwally Mahmoud, Ali MH Al Thaiban, Abdulwasa B. Barnawi, Zakaria M. Salem Elbarbary, Ahmed Ibrahim Omar, and HanyAbdelfattah. "Operation of grid-connected PV system with ANN-based MPPT and an optimized LCL filter using GRG algorithm for enhanced power quality." IEEE Access 11 (2023): 106859-106876.

[20] Alemu, Yechale Amogne, Belachew Bantyirga Gessesse, and Molla Addisu Mossie. "Transient stability enhancement using adaptive neuro-fuzzy-based unified power flow controller." Scientific African 24 (2024): e02195.

[21] Çelik, Doğan, and Hafiz Ahmed. "Enhanced control of superconducting magnetic energy storage integrated UPQC for power quality improvement in EV charging station." Journal of Energy Storage 62 (2023): 106843.

[22] Srimatha, S., Balasubbareddy Mallala, and J. Upendar. "A novel ANFIS-controlled customized UPQC device for power quality enhancement." Journal of Electrical Systems and Information Technology 10, no. 1 (2023): 55.

[23] Mahar, Hina, Hafiz Mudasir Munir, Jahangir BadarSoomro, FaheemAkhtar, Rashid Hussain, Mohamed F. Elnaggar, Salah Kamel, and Josep M. Guerrero. "Implementation of ANN Controller Based UPQC Integrated with Microgrid." Mathematics 10, no. 12 (2022): 1989.

[24] Zanib, Noor, MuniraBatool, SaleemRiaz, and Fawad Nawaz. "Performance analysis of renewable energy based distributed generation system using ANN TUNED UPQC." IEEE Access 10 (2022): 110034-110049.
[25] Lei, Tongfei, SaleemRiaz, Noor Zanib, MuniraBatool, Feng Pan, and Shaoguo Zhang. "Performance analysis of grid-connected distributed generation system integrating a hybrid wind-PV farm using UPQC." Complexity 2022 (2022).

Information about authors.

Mr.Chindam Anilkumar,
Research Scholar,
Department of Electrical and Electronics Engineering,
Annamalai University,
Tamil Nādu, India, 608002.
The field of scientific Interest is Power Distribution System.
E-mail:
aniljntuhcej@gmail.com

Mr.IlanjiAkilandam Chidambaram,
Professor,
Department of Electrical and Electronics Engineering.
Annamalai University,
Tamilnadu, India -608002.
Field of scientific interest is Power Quality in Electrical Distribution systems, E-mail:
driacdm@gmail.com

Mr.Venugopal Dugyala,
Associate Professor,
Department of Electrical and Electronics Engineering,
Kamala Institute of Technology and Science,
Telangana, India-505468.
Field of Scientific interest is power electronics applications in power systems.
Email: venufacts20m@gmail.com